Report of the project

Title of Project: Highly potent dual-targeting angiotensin-converting enzyme 2 (ACE2) and neuropilin-1 (NRP1) peptides: a promising broad-spectrum therapeutic strategy against SARS-CoV-2 infection

Project Source

Sponsored by: _____

Conducted by: Nanjing Junling Smart Medicine Biotech Co., Ltd.

Completion Date: 2022.06

Highly Potent Dual-Targeting Angiotensin-Converting Enzyme 2 (ACE2) and Neuropilin-1 (NRP1) Peptides: A Promising Broad-Spectrum Therapeutic Strategy against SARS-CoV-2 Infection

Executive Summary

We used a novel screening protocol that combined docking based on the ACE2 pharmacophore model with molecular dynamics (MD) simulations, resulting in potential dual-targeting ACE2/NRP1 peptides. These potential peptides were then synthesized for binding affinity, anti-pseudovirus infection, and cytotoxicity assays.

Introduction

Coronavirus disease 2019 (COVID-19), caused by severe acute respiratory syndrome coronavirus 2 (SARS-CoV-2), has become a major common health issue resulting in more than 765 million diagnosed cases and over 6.9 million deaths globally.[1-3] The blockade of viral entry is one of the most effective ways to fight the infection.[4, 5] The type I transmembrane metallocarboxypeptidase angiotensin-converting enzyme 2 (ACE2) is the pivotal entry receptor of SARS-CoV-2.[6, 7] ACE2 can be recognized and engaged by the receptor-binding domain (RBD) of SARS-CoV-2 S proteins, allowing the virus to enter host cells.[8, 9] In addition, the transmembrane glycoprotein neuropilin-1 (NRP1) was reported to serve as another factor in favor of SARS-CoV-2 entry.[10, 11] According to SARS-CoV-2 pseudovirus entry assays, the expression of NRP1 alone did not promote SARS-CoV-2 infection, but its coexpression with ACE2 markedly enhanced it.[10] Consequently, simultaneous inhibition of ACE2 and NRP1 may be a more effective and complementary approach, which may exert not only broad-spectrum but also synergistic inhibition to reduce viral infection and prevent relevant disorders (Figure 1).

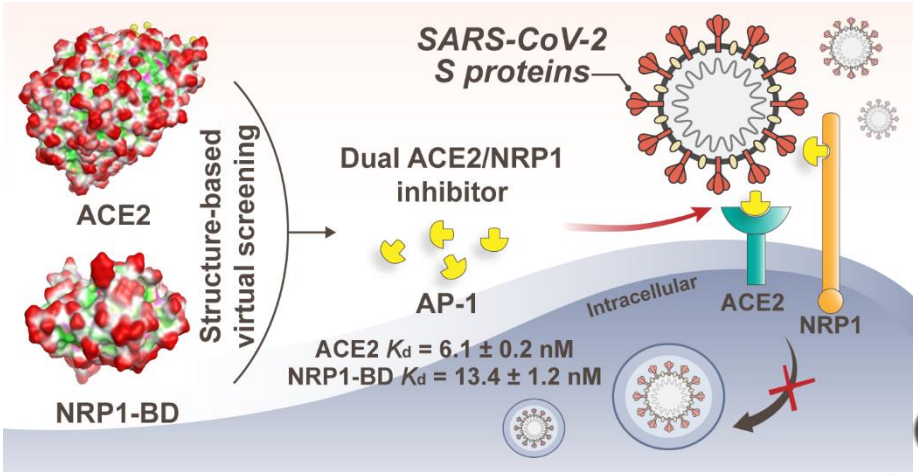

Figure 1. Schematic depicting the mechanism by which dual-targeting ACE2/NRP1 inhibitors suppress SARS-CoV-2 infection.

Experimental and Results

Virtual screening for peptides that target both ACE2 and NRP1

The crystal structure of SARS-CoV-2 RBD and human ACE2 complex (PDB ID: 7DQA) was retrieved from the PDB database (http://www.rcsb.org). All virtual screening operations were performed in the Molecular Operating Environment program (MOE, Chemical Computing Group Inc, Montreal, Quebec, Canada). The crystal structure was imported into the program and processed using the Structure Preparation Tool. Based on crucial hydrogen-bond interactions enabling SARS-CoV-2 to bind to ACE2, the Pharmacophore Query Editor was used to manually elucidate the 3D pharmacophore model of ACE2. As shown in Figure 2A, the final pharmacophore model of ACE2 was composed of these five features, namely one hydrogen-bond donor feature (F1, pink color) and four hydrogen-bond acceptor features (F2–F5, yellow color).

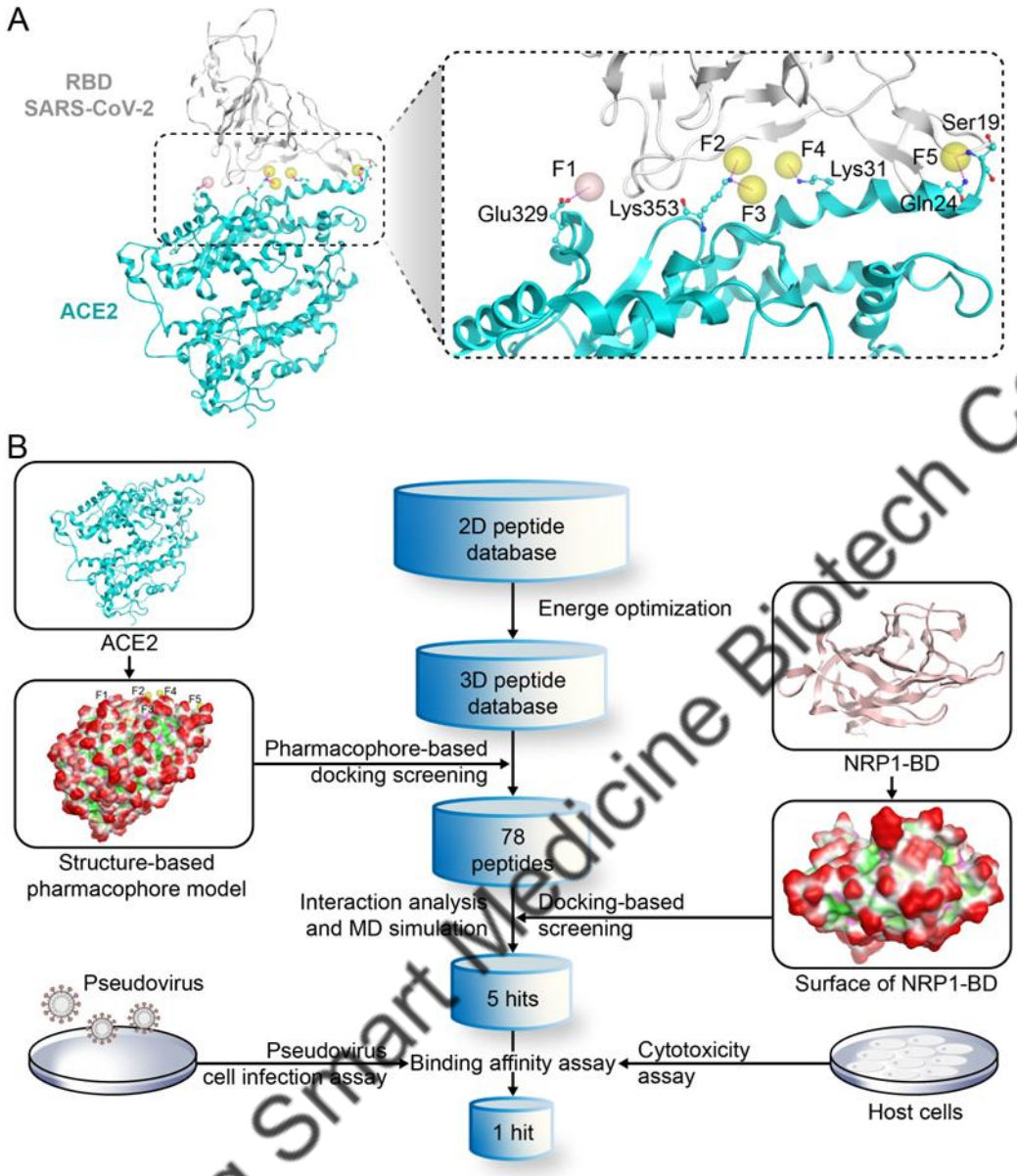

Figure 2. Structure-based virtual screening for peptides that target both ACE2 and NRP1. (A) Feature details of the ACE2 pharmacophore model (F1: hydrogen-bond donor feature; F2–F5: hydrogen-bond acceptor features). (B) The flowchart of a screening protocol for discovering dual ACE2/NRP1 inhibitors. Spheres were utilized to depict ACE2 pharmacophore features. Purple dotted lines were used to present hydrogen bonds. The secondary structures of protein were displayed as lines. The polar (purple), exposed (red), and hydrophobicity (green) areas of the ACE2 and NRP1-BD surfaces were plotted.

Figure 2B depicts a schematic flowchart of the virtual screening procedure and some bioassays applied in this study. Firstly, we built a virtual database containing

32,000 peptides. An energy optimization protocol was used to convert the two-dimensional (2D) structures of a total of 32,000 peptides in the database to 3D structures. The pharmacophore-based docking was then performed using the ACE2 pharmacophore model as a probe to identify ACE2-targeting peptides, and docking scores were calculated. This pharmacophore-based docking strategy can ensure that peptides sufficiently bind to the RBD-binding interface of ACE2. As a result, a total of 78 peptides were obtained by setting the reasonable docking score threshold of < −8.94 kcal/mol and adopted for the following screening of NRP1-targeting hits. Thus, ACE2-targeting peptides were subjected to docking into NRP1-BD, whose crystal structure was retrieved from PBD, to find dual ACE2/NRP1-targeting inhibitors. The top-ranked peptides were screened out, and the top five peptides (APs 1–5) that potentially targeted both ACE2 and NRP1 were selected for subsequent interaction analysis and MD simulations. Docking scores and structures of APs 1–5 are shown in Table S1 and Figure S3, respectively.

Table S1. The docking scores of the screened peptides

	ACE2	NRP1-BD
Name	Binding free energy[a] (kcal/mol)	Binding free energy (kcal/mol)
AP-1	−14.09	−13.66
AP-2	−13.72	−12.12
AP-3	−13.65	−13.27
AP-4	−13.69	−12.61
AP-5	−13.63	−13.31
$S_{471–503}$	−8.94	/
NMTP-5	/	−11.86

[a]Binding free energy between the peptide and the target (lower binding free energies suggest stronger binding affinities).

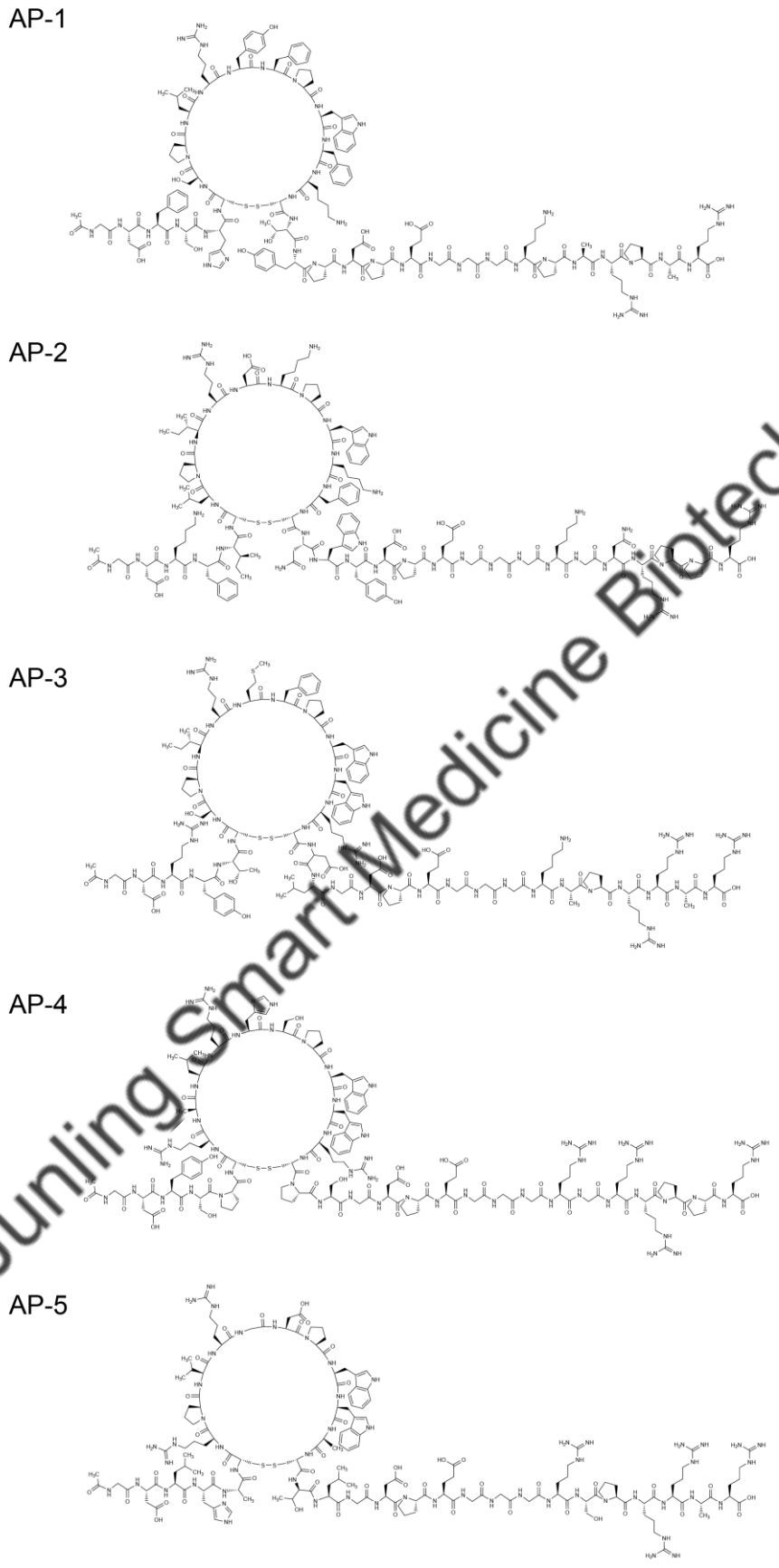

Figure S3. The structures of APs 1–5.

Interaction analysis

To investigate how the five hits interact with the binding sites, ACE2- and NRP1-based docking were performed, respectively. The crystal structure of APs 1–5 and ACE2 complexes and the crystal structure of APs 1–5 and NRP1 complexes were constructed in a molecular operating environment (MOE). The above crystal structures are prepared using MOE's QuickPrep tool. Then, the Amber14: EHT force field is set to minimize the crystal structure energy. Based on the above crystal structures, the interaction between the crystal structures of APs 1–5 and ACE2 complexes and the crystal structures of APs 1–5 and NRP1 complexes was analyzed using the Ligand Interactions tool in MOE.

As shown in Figure 3, with their rigid cyclic structure, all the hits matched the five pharmacophoric features of ACE2. Among them, AP-1 and AP-2 overlaid onto the whole features more completely as the =N of guanidine of C-end arginine overlapped well with the F1 annotation point (Figures 3A and 3C). Notably, all the hits were found to interact with key residues corresponding to the F1–F5 features, namely Glu329, Lys353, Lys31, Gln24, and Ser19, contributing to specific ACE2-binding with a higher number of hydrogen bonds than anticipated (Figure 3). Moreover, several hydrogen-bond interactions with other residues were observed, such as Asp38, Leu351, Glu35, Phe28, Glu75, Gln76, Gly352, and Glu37. Residues Asp38 and Leu351 of ACE2 were only found to form hydrogen bonds with the lysine branch near the C-end of AP-1 and AP-2 (Figures 3A and 3C). The hydrogen bonds formed by the residues Glu35 and Phe28 of ACE2 were only displayed in AP-1 (Figure 3A). The residue Glu75 was only involved in hydrogen-bond interaction with AP-2 due to the -$NH3^+$ group of the lysine side chain (Figure 3C). The residue Gln76 of ACE2 was discovered to establish hydrogen-bond interactions in AP-1, AP-3, and AP-4 (Figures 3A and 3D–3E). A

hydrogen bond formed with residue Gly352 was found in AP-3, AP-4, and AP-5 (Figures 3D–3F). In AP-4 and AP-5, a hydrogen bond formed with residue Glu37 was also found (Figures 3E–3F). As depicted in Figure 3B, although the ACE2 binding surface is wide with some shallow depressions, AP-1 can still embed into it properly.

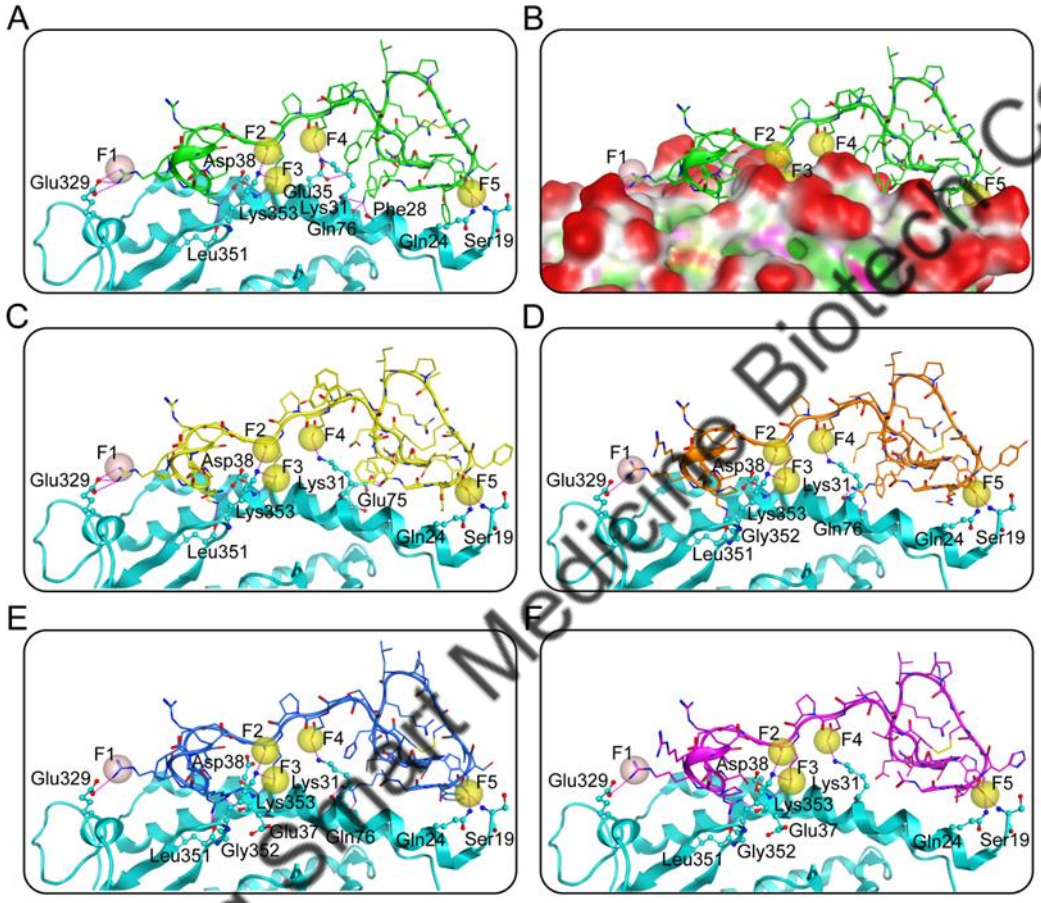

Figure 3. Docking poses predicted for APs 1–5 at the RBD binding site of ACE2. (A) and (B) represented the predicted binding mode of AP-1. (C)–(F) represented the predicted binding modes of APs 2–5, respectively. Different colors were used to indicate hits (green for AP-1, yellow for AP-2, orange for AP-3, dark blue for AP-4, and purple for AP-5), and cyan-blue was used to color the ACE2 protein. Spheres were utilized to depict ACE2 pharmacophore features. Purple dotted lines were used to present hydrogen bonds. The secondary structures of protein were displayed as lines. The polar (purple), exposed (red), and hydrophobicity (green) areas of the ACE2 and NRP1-BD surfaces were plotted.

Figure 4 illustrates the binding modes of the five hits within the NRP1 active site.

The four amino-acid residues at the C-end of all hits played a major role in binding to NRP1. They formed hydrogen-bond interactions with NRP1 residues, which are critical for the SARS-CoV-2 binding, including Glu319, Tyr297, Trp301, Asp320, Ile415, Tyr353, Ser346, and Thr349.[11, 12] In particular, the C-end residue arginine of hits exhibited seven hydrogen bonds with residues Try301, Asp320, Ile415, Tyr353, Ser346, and Thr349 of NRP1, leading to tightly binding to NRP1-BD (Figures 4A, 4C–4F). Additionally, the oxygen atom on the acetyl group at the N-end glycine of hits was engaged in the hydrogen-bond interaction with NRP1 residue Ala293. Some hydrogen bonds were only found in individual hits, for instance, one hydrogen bond formed by Glu367 was shown in AP-1 (Figure 4A), and the other formed by Gln296 was only exhibited in AP-2 (Figure 4C). The hydrogen-bond interaction formed by residue Gly366 was present in both AP-3 and AP-5 (Figures 4D and AF). The binding surface of AP-1 to NRP1-BD is illustrated in Figure 4B, the C-end residues of AP-1 were able to access the pocket of the b1 domain, enhancing the binding performance. The ring part of all hits showed few interactions with NRP1.

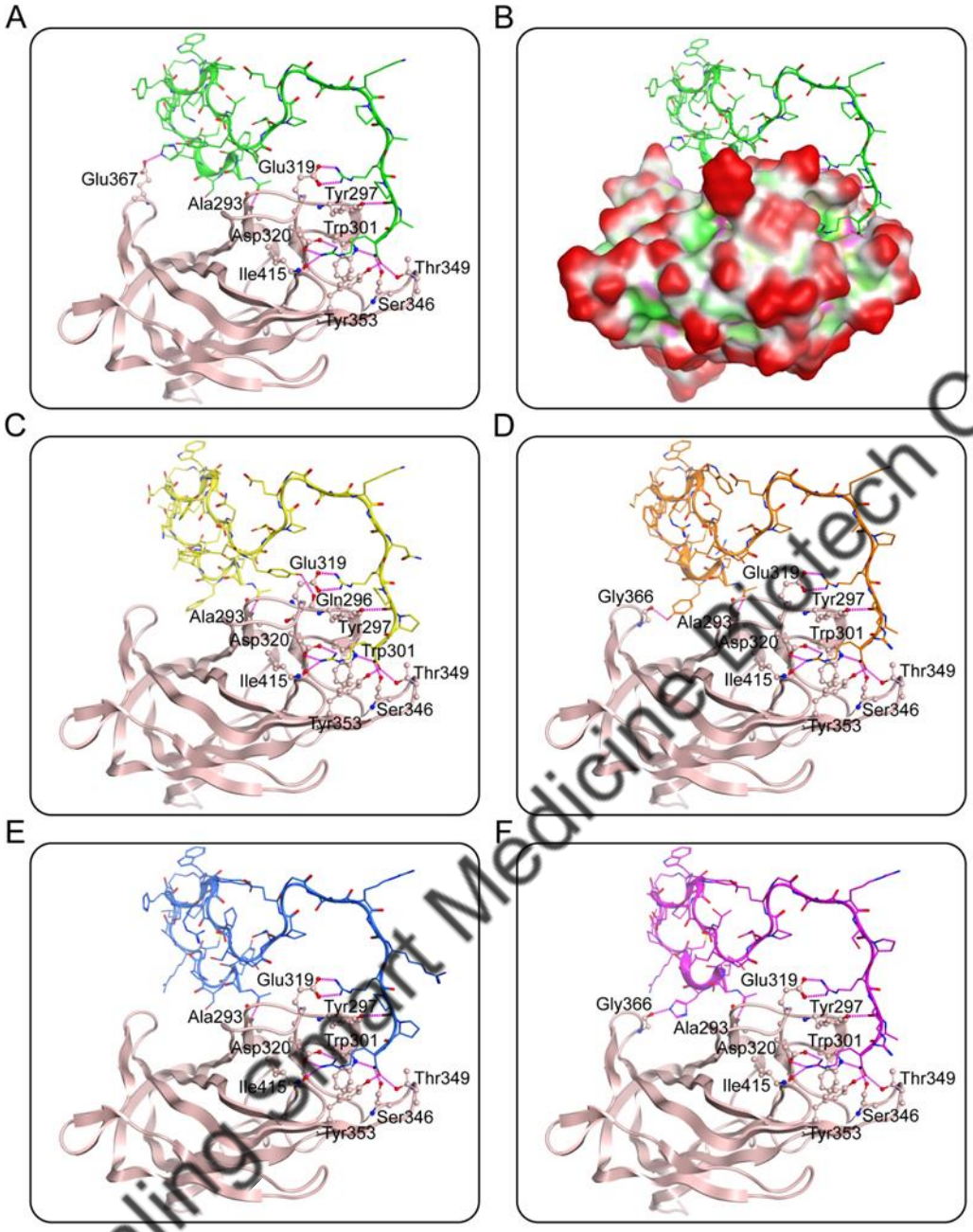

Figure 4. Docking poses predicted for APs 1–5 at NRP1-BD. (A) and (B) represented the predicted binding mode of AP-1. (C)–(F) represented the predicted binding modes of APs 2–5, respectively. Different colors were used to indicate hits (green for AP-1, yellow for AP-2, orange for AP-3, dark blue for AP-4, and purple for AP-5), and pink was used to color the NRP1-BD protein. Purple dotted lines were used to present hydrogen bonds. The secondary structures of protein were displayed as lines. The polar (purple), exposed (red), and hydrophobicity (green) areas of the ACE2 and NRP1-BD surfaces were plotted.

Molecular dynamics (MD) simulations

All MD simulations were carried out in GROMACS 2019.4 using the force fields of AMBER99SB-ILDN. The best binding modes of ACE2-hit and NRP1-hit complexes were obtained from the docking results and subjected to MD simulations. Each complex system was solvated in a cube (1.0 nm in diameter) with water molecules modeled as extended simple point charges (SPC/E). For neutralizing the systems, counter ions (sodium and chloride ions) were added. Then, energy minimization was performed via the method of steepest descent. Afterward, equilibrations of NVT (1 bar) and NPT (300 K) were conducted for 100 ps each. Eventually, 100 ns MD simulations were implemented, and conformations were stored every 100 ps. The secondary-structure analysis was carried out by DSSP (Dictionary of Secondary Structure for Proteins).

By docking-based virtual screening, five hits with dual ACE2/NRP1-binding potential were identified. To further test the binding stability of ACE2-hit and NRP1-hit complexes, 100 ns MD simulations were carried out. The results of root-mean-square deviations (RMSDs) of the complexes and root-mean-square fluctuations (RMSFs) of ACE2/NRP1 residues showed a stable binding between the five hits and ACE2/NRP1 (Figure S4 and S5). Furthermore, the secondary-structure contents of ACE2 and NRP1 also remained almost unchanged during the simulation time (Figure S6). Taken together, these docking and MD results suggest that APs 1–5 have the potential to interact with crucial site residues of ACE2 and NRP1 with good binding stability.

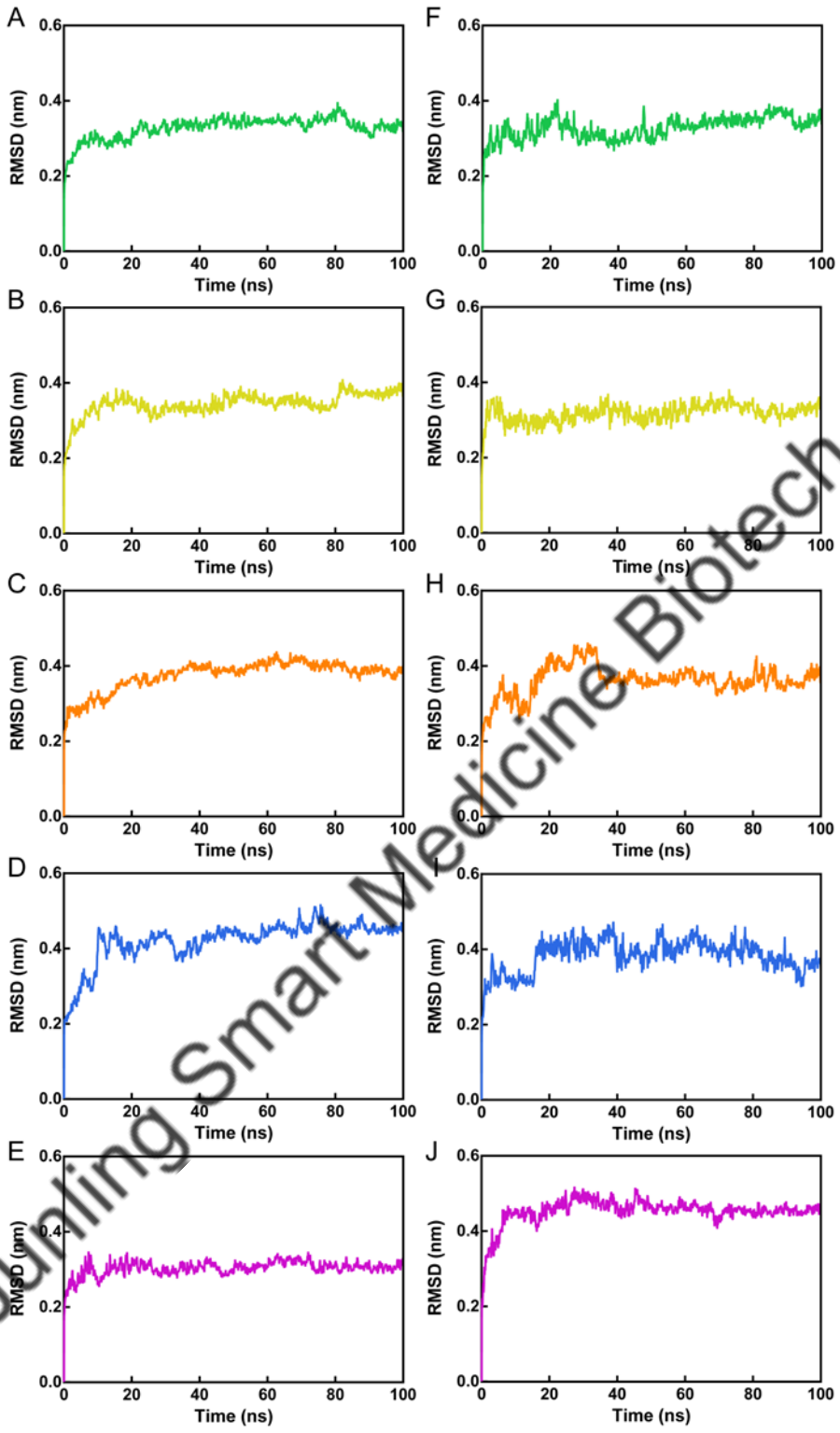

Figure S4. RMSD of ACE2-hit and NRP1-hit complexes with respect to the initial structures obtained from docking. (A–E) RMSD in ACE2-hit complexes, and (F–J) RMSD in NRP1-hit complexes. In all panels the color code is AP-1 (green), AP-2 (yellow), AP-3 (orange), AP-4 (dark blue), and AP-5 (purple).

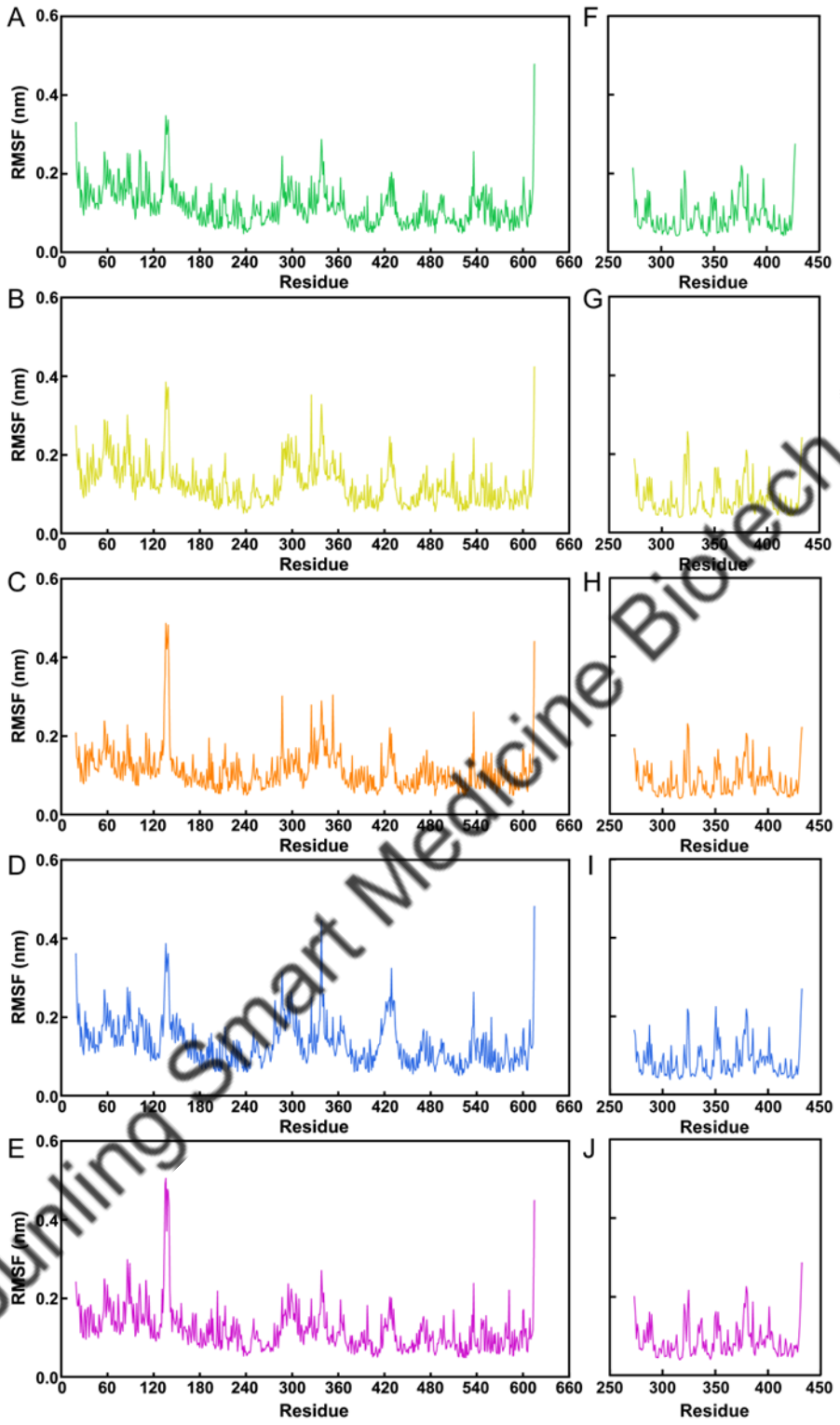

Figure S5. RMSF of residues of the ACE2 protein in ACE2-hit complexes (A–E) and the NRP1-BD protein in NRP1-hit complexes (F–J). In all panels the color code is AP-1 (green), AP-2 (yellow), AP-3 (orange), AP-4 (dark blue), and AP-5 (purple).

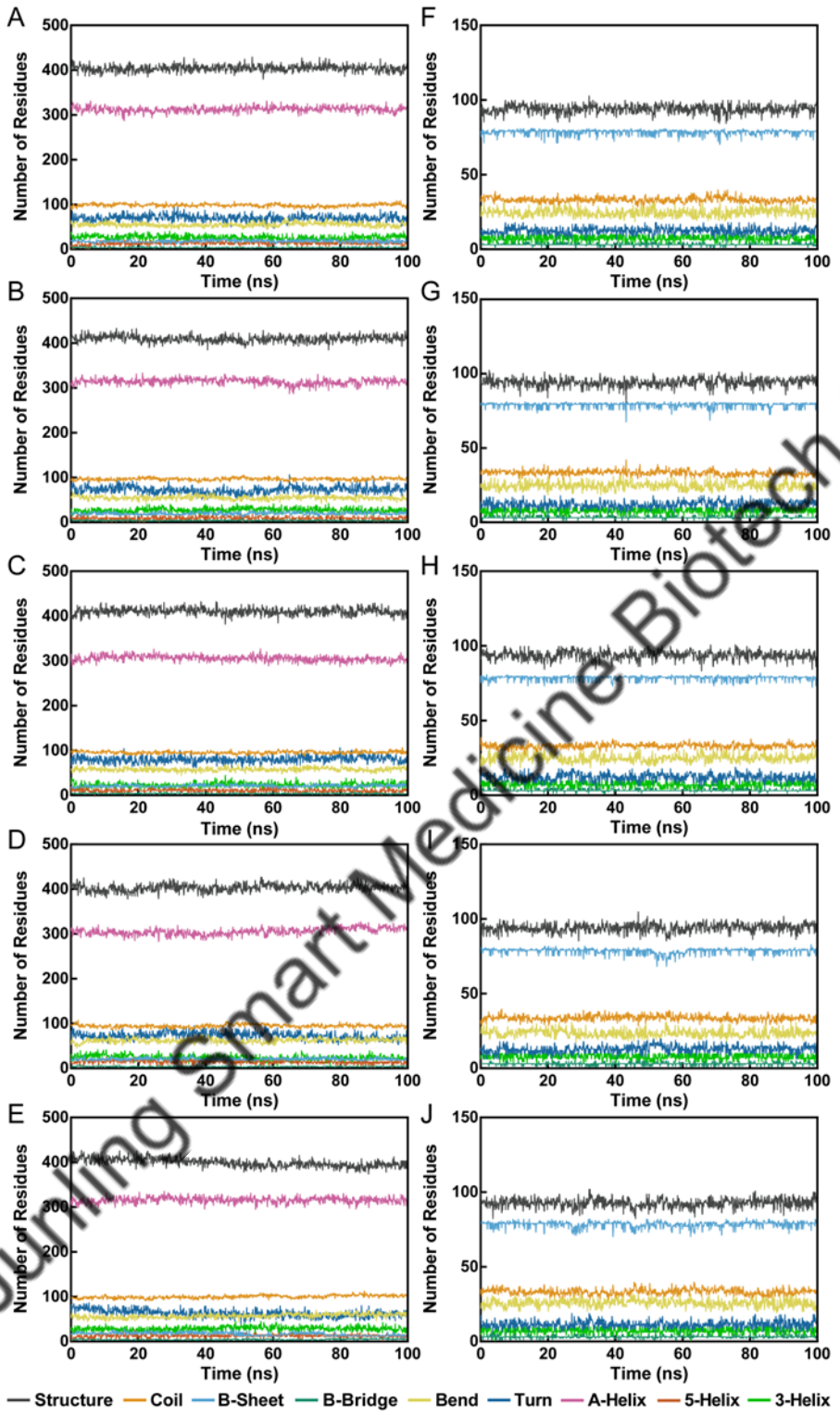

Figure S6. The secondary-structure contents of the ACE2 protein in ACE2-hit complexes (A–E) and the NRP1-BD protein in NRP1-hit complexes (F–J). Herein: (A) and (F) indicate AP-1 complexes, (B) and (G) indicate AP-2 complexes, (C) and (H) indicate AP-3 complexes, (D) and (I) indicate AP-4 complexes, and (E) and (J) indicate AP-5 complexes.

Identification of peptides

Microscale thermophoresis (MST) analysis was applied to examine peptide binding ability. For visible detection of ACE2 and NRP1 proteins in this study, Lys labeling kits were purchased for labeling. With a Monolith NT.115 instrument (20 % LED, 50 % MST power), all measurements were taken in standard-prepared capillaries. Subsequent detailed operations were carried out as described previously.[13]

To evaluate the binding ability of APs 1–5 to ACE2 and NRP1, we first used the microscale thermophoresis (MST) method. As shown in Figure 5A and Figure S7, APs 1–5 had strong binding affinities to ACE2 and NRP1, with values in the range from 6.1 to 101.2 nM and 13.4 to 96.7 nM, respectively. Among them, AP-1 was the most potent peptide targeting ACE2 (K_d = 6.1 ± 0.2 nM) and NRP1 (K_d = 13.4 ± 1.2 nM). In addition, we also evaluated the ability of ACE2- and NRP1-positive inhibitors $S_{471–503}$ and NMTP-5 to bind to ACE2 and NRP1 proteins, respectively.[14, 15] As a positive control for ACE2 inhibitor, we discovered that $S_{471–503}$ had a binding affinity for ACE2 (K_d = 621.9 ± 12.8 nM), but nearly no binding affinity for NRP1. Similarly, NMTP-5, as a positive control for NRP1 inhibitor, showed a binding affinity for NRP1-BD with K_d = 105.6 ± 4.7 nM, but almost no binding affinity for ACE2 (Figure 5A). Compared with the single target inhibitors $S_{471–503}$ and NMTP-5, the binding affinity of AP-1 was significantly increased by approximately 102-fold for ACE2 and 8-fold for NRP1.

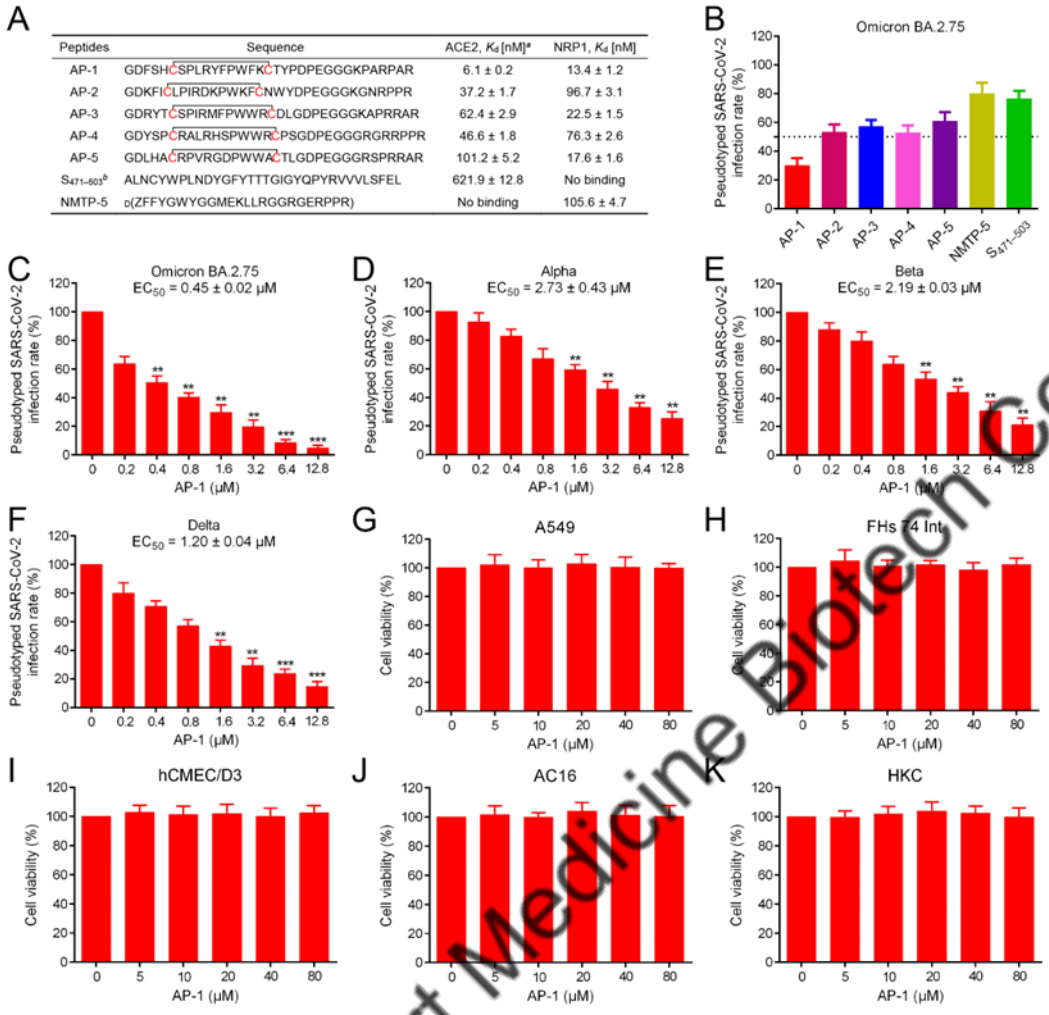

Figure 5. Biological assays of peptides. (A) Peptide sequences as well as their binding affinities for ACE2 and NRP1 proteins. [a]MST data. [b]$S_{471–503}$ was used as a positive ACE2 inhibitor and NMTP-5 served as a positive NRP1 inhibitor. The N-terminus of APs 1–5 was acetylated. Each peptide was cyclized via a disulfide link generated by two cysteines. (B) Effect of screened peptides APs 1–5, $S_{471–503}$, and NMTP-5 at a concentration of 1.6 μM on the infection rate of pseudotyped SARS-CoV-2 Omicron BA.2.75 in 293T-ACE2$^+$/NRP1$^+$ cells. (C)–(F) Dose-dependent (0–12.8 μM) assay of AP-1 on different SARS-CoV-2 variants. (G)–(K) The MTT assay was employed to detect the cytotoxicity of AP-1. Cells were processed with a range of peptide concentrations (0–80 μM) for 48 hours. The results are represented as mean ± SD (n = 3), **P < 0.01, ***P < 0.001 versus the control group.

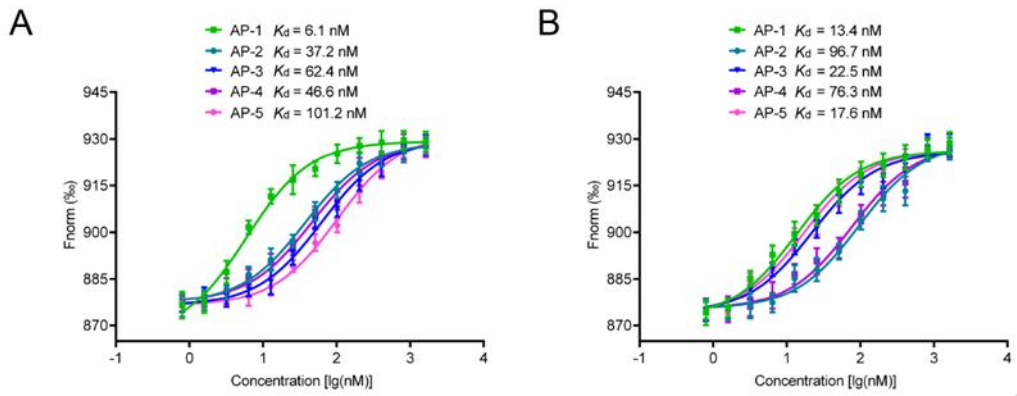

Figure S7. Binding affinity (K_d) graphs of APs 1–5 for ACE2 (A) and NRP1 (B) were determined using MST.

Inhibition of pseudotyped SARS-CoV-2 infection

Pseudoviruses in this experiment were produced from pseudotyped HIV-1 viruses, and the S proteins of Omicron BA.2.75, Alpha, Beta, and Delta were expressed on their surfaces. Also, to detect visually, the firefly luciferase gene was included. The cells used here were 293T-ACE2$^+$/NRP1$^+$ cells or 293T-ACE2$^+$/NRP1$^-$ cells with a density of 2 × 10^4 per well, which were seeded onto 96-well plates and incubated overnight at 37 °C in a 5% (v/v) CO_2 atmosphere. Percentage of infection rate (%) was calculated by (luminescence signal of the test sample)/(luminescence signal of negative control sample) × 100. The same follow-up manipulations were taken according to our previous study.[13]

Research on SARS-CoV-2 is difficult and dangerous due to the high infectivity and pathogenicity of SARS-CoV-2.[16] Pseudovirus is a highly secure, host-broad, and genetically stable system suitable as a safe and effective alternative to SARS-CoV-2 entry assays.[10, 17-19] Furthermore, good concordance of neutralization assays between pseudovirus and SARS-CoV-2 has been reported in previous studies.[20] Thus, we tested the anti-infective activities of APs 1–5 against SARS-CoV-2 pseudoviruses. The

cytotoxicity of APs 1–5 was first evaluated. At a concentration of 20 μM, APs 1–5 had little impact on the viability of 293T-ACE2^{+}/NRP1^{+} cells (Figure S8). We then carried out the pseudovirus entry assay under this nontoxic concentration. As illustrated in Figure 5B, five peptides showed stronger anti-infective activities against the SARS-CoV-2 Omicron BA.2.75 pseudovirus than positive controls $S_{471–503}$ and NMTP-5 at a concentration of 1.6 μM. Particularly, AP-1 was evaluated as the potent agent with about 70% inhibition against Omicron BA.2.75 infection. Further experiments showed that the corresponding EC_{50} values of AP-1 on different pseudovirus including Omicron BA.2.75, Alpha, Beta, and Delta were 0.45, 2.73, 2.19, and 1.20 μM, respectively (Figures 5C–5F). We also conducted this assay in 293T-ACE^{+}/NRP1^{-} cells and found that APs 1–5 exhibited better inhibitory effects on pseudotyped SARS-CoV-2 Omicron BA.2.75 infection compared with the positive controls (Figure S9). Among them, AP-1 showed the strongest inhibitory effect. The results indicate that AP-1 possesses antiviral activity against different VOCs of SARS-CoV-2, and importantly, the observed inhibitory activity is relevant to the simultaneous inhibition of both ACE2 and NRP1, which aligns with our initial hypothesis for designing dual-target inhibitors.

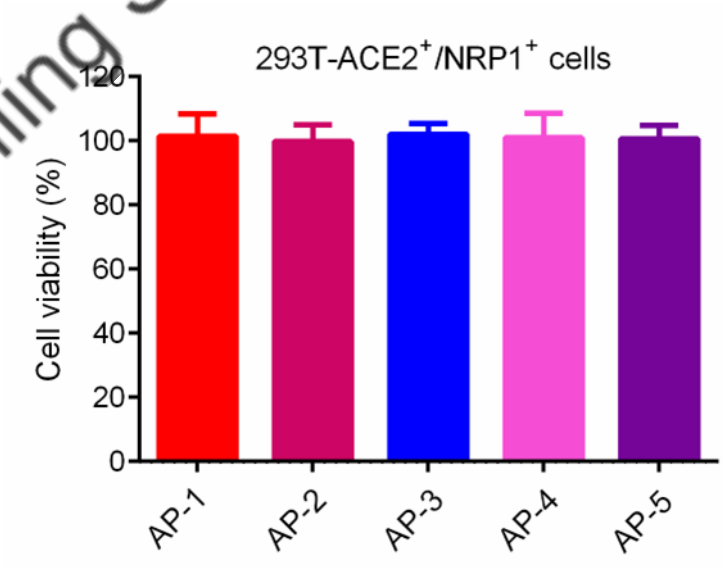

Figure S8. The cytotoxicity effects of APs 1–5 on 293T-ACE2^{+}/NRP1^{+} cells using the MTT assay.

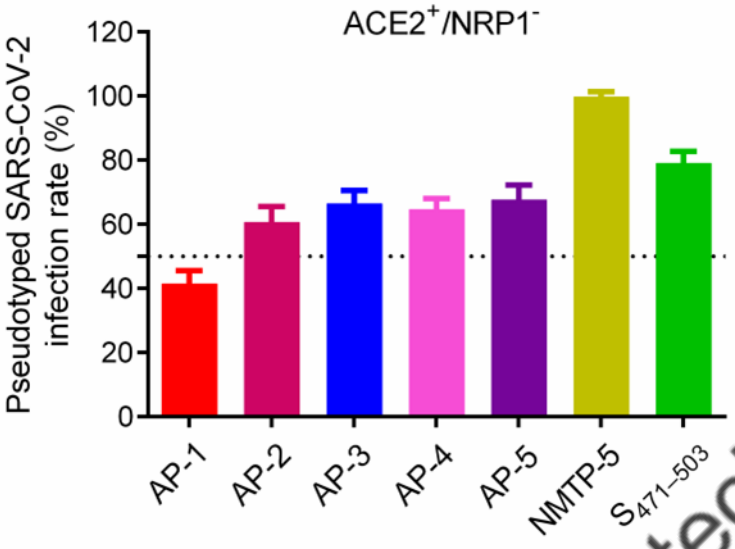

Figure S9. Effect of screened peptides APs 1–5, $S_{471–503}$, and NMTP-5 at a concentration of 1.6 μM on the infection rate of pseudotyped SARS-CoV-2 Omicron BA.2.75 in 293T-ACE2$^+$/NRP1$^-$ cells.

Cytotoxicity of AP-1

Cell cytotoxicity was measured using MTT assays. A549, FHs 74 Int, hCMEC/D3, AC13, and HKC cells were seeded at a concentration of 5 × 10^4 cells per well in 96-well plates, and their incubation was carried out overnight at 37 °C under 5% (v/v) CO_2 atm. Then, peptides with varied concentrations were used to process the cells. The specific steps of MTT assays referred to the procedures in our published study.[21]

The loss of membrane integrity in dead cells allows for the permeation of trypan blue (TB) dye into the cells, while alive cells have intact cell membranes that prevent penetration of TB. Based on this principle, the trypan blue assay that distinguishes between dead and alive cells was used to determine the cytotoxicity of peptides. The specific steps for the trypan blue assay referred to the procedures in previously published studies.[22]

As mentioned above, besides pulmonary manifestations as the main symptom, there are many extrapulmonary symptoms in COVID-19 patients, and SARS-CoV-2 was found in the organs corresponding to these symptoms, such as the intestine, brain, heart, and kidney.[23, 24] Moreover, the 293T-ACE2^{+}/NRP1^{+} cells used in the pseudovirus anti-infection assay were unable to represent the toxicity of peptides to host cells.[25] Hence, to further explore the cytotoxicity of AP-1, some human normal cells were used, including human pulmonary alveolar basal epithelial cells (A549), human fetal small intestinal epithelial cells (FHs 74 Int), human brain endothelial cell line (hCMEC/D3), human cardiomyocyte cells (AC16), and renal tubular epithelial cells (HKC). After treating the cells with different concentrations, the viability of AP-1 in these cells was not affected in a dose-dependent manner (Figures 5G–5K). Importantly, AP-1 did not show any observable cytotoxicity even at the high concentration of 80 μM, demonstrating the excellent safety of AP-1. Further results of trypan blue staining also confirmed the non-toxicity of APs 1–5 (Figure S10). Collectively, these data demonstrate that peptide AP-1 has high antiviral potency with no obvious toxicity.

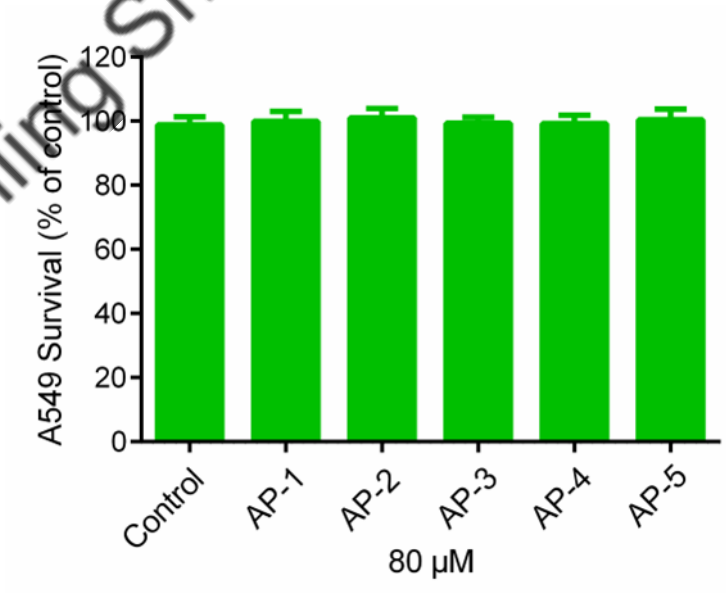

Figure S10. Cell death assay by trypan blue staining.

Conclusion

The continuous emergence of SARS-CoV-2 VOCs has been an enormous danger to global health and a considerable challenge to the development of COVID-19 therapeutics. However, host-directed antivirals provide insights into the pan-inhibition of SARS-CoV-2. Here, we proposed a novel therapeutic strategy simultaneously targeting ACE2 and NRP1, two crucial host receptors for viral entry, instead of neither their alone nor RBD, which may allow us to bypass emerging VOCs with extraordinary anti-infective efficacy. Through a combined virtual screening approach and MD simulations, five potential dual-targeting ACE2/NRP1 peptides were identified. The AP-1 among them exhibited the most potent inhibitory activity with a nanomolar range binding affinity to both ACE2 and NRP1 and was several times higher than that of the positive controls. The antiviral efficacy was further favored by infection assays of SARS-CoV-2 pseudoviruses and cytotoxicity assays in host cells. AP-1 showed remarkable entry prevention of SARS-CoV-2 VOCs without impairing host cell viability. In conclusion, AP-1 as a highly potent dual ACE2/NRP1-targeting agent has the potential for broad-spectrum inhibition against SARS-CoV-2 infection, and in the future, this novel therapeutic strategy may serve as a powerful weapon to confront emerging SARS-CoV-2 VOCs.

References

(1) Wu, F.; Zhao, S.; Yu, B.; Chen, Y.-M.; Wang, W.; Song, Z.-G.; Hu, Y.; Tao, Z.-W.; Tian, J.-H.; Pei, Y.-Y.; et al. A new coronavirus associated with human respiratory disease in China. *Nature* **2020**, *579* (7798), 265-269.

(2) *Coronavirus disease (COVID-19)*. https://www.who.int/health-topics/coronavirus (accessed 2023-03-13).

(3) *Weekly epidemiological update on COVID-19 - 10 August 2022*. https://www.who.int/publications/m/item/weekly-epidemiological-update-on-covid-19---8-march-2023 (accessed 2023-03-13).

(4) Xiu, S.; Dick, A.; Ju, H.; Mirzaie, S.; Abdi, F.; Cocklin, S.; Zhan, P.; Liu, X. Inhibitors of SARS-CoV-2 entry: current and future opportunities. *J. Med. Chem.* **2020**, *63* (21), 12256-12274.

(5) Twomey, J. D.; Luo, S.; Dean, A. Q.; Bozza, W. P.; Nalli, A.; Zhang, B. COVID-19 update: The race to therapeutic development. *Drug Resistance Updates* **2020**, *53*, 100733.

(6) Hoffmann, M.; Kleine-Weber, H.; Schroeder, S.; Krüger, N.; Herrler, T.; Erichsen, S.; Schiergens, T. S.; Herrler, G.; Wu, N.-H.; Nitsche, A. SARS-CoV-2 cell entry depends on ACE2 and TMPRSS2 and is blocked by a clinically proven protease inhibitor. *Cell* **2020**, *181* (2), 271-280.

(7) Walls, A. C.; Park, Y.-J.; Tortorici, M. A.; Wall, A.; McGuire, A. T.; Veesler, D. Structure, function, and antigenicity of the SARS-CoV-2 spike glycoprotein. *Cell* **2020**, *181* (2), 281-292.

(8) Wrapp, D.; Wang, N.; Corbett, K. S.; Goldsmith, J. A.; Hsieh, C.-L.; Abiona, O.; Graham, B. S.; McLellan, J. S. Cryo-EM structure of the 2019-nCoV spike in the prefusion conformation. *Science* **2020**, *367* (6483), 1260-1263.

(9) Yan, R.; Zhang, Y.; Li, Y.; Xia, L.; Guo, Y.; Zhou, Q. Structural basis for the recognition of SARS-CoV-2 by full-length human ACE2. *Science* **2020**, *367* (6485), 1444-1448.

(10) Cantuti-Castelvetri, L.; Ojha, R.; Pedro, L. D.; Djannatian, M.; Franz, J.; Kuivanen, S.; van der Meer, F.; Kallio, K.; Kaya, T.; Anastasina, M. Neuropilin-1 facilitates SARS-CoV-2 cell entry and infectivity. *Science* **2020**, *370* (6518), 856-860.

(11) Daly, J. L.; Simonetti, B.; Klein, K.; Chen, K.-E.; Williamson, M. K.; Antón-Plágaro, C.; Shoemark, D. K.; Simón-Gracia, L.; Bauer, M.; Hollandi, R. Neuropilin-1 is a host factor for SARS-CoV-2 infection. *Science* **2020**, *370* (6518), 861-865.

(12) Perez-Miller, S.; Patek, M.; Moutal, A.; Duran, P.; Cabel, C. R.; Thorne, C. A.; Campos, S. K.; Khanna, R. Novel compounds targeting neuropilin receptor 1 with potential to interfere with SARS-CoV-2 virus entry. *ACS Chem. Neurosci.* **2021**, *12* (8), 1299-1312.

(13) Yin, S.; Mei, S.; Li, Z.; Xu, Z.; Wu, Y.; Chen, X.; Liu, D.; Niu, M.-M.; Li, J. Non-covalent cyclic peptides simultaneously targeting Mpro and NRP1 are highly effective against Omicron BA. 2.75. *Front. Pharmacol.* **2022**, *13*, 1037993.

(14) Hu, H.; Li, L.; Kao, R. Y.; Kou, B.; Wang, Z.; Zhang, L.; Zhang, H.; Hao, Z.; Tsui, W. H.; Ni, A. Screening and identification of linear B-cell epitopes and entry-blocking peptide of severe acute respiratory syndrome (SARS)-associated coronavirus using synthetic overlapping peptide library. *J. Comb. Chem.* **2005**, *7* (5), 648-656.

(15) Zhou, Y.; Chen, Y.; Tan, Y.; Hu, R.; Niu, M. M. An NRP1/MDM2-targeted D-peptide supramolecular nanomedicine for high-efficacy and low-toxic liver cancer therapy. *Adv. Healthcare Mater.* **2021**, *10* (9), 2002197.

(16) Chen, M.; Zhang, X.-E. Construction and applications of SARS-CoV-2 pseudoviruses: a mini

review. *Int. J. Biol. Sci.* **2021**, *17* (6), 1574-1580.
(17) Xiang, Q.; Li, L.; Wu, J.; Tian, M.; Fu, Y. Application of pseudovirus system in the development of vaccine, antiviral-drugs, and neutralizing antibodies. *Microbiol. Res.* **2022**, *258*, 126993.
(18) Voytas, D. F. Pseudoviruses. In *Encyclopedia of Virology*, Elsevier Ltd, 2008; pp 352-357.
(19) Neerukonda, S. N.; Vassell, R.; Herrup, R.; Liu, S.; Wang, T.; Takeda, K.; Yang, Y.; Lin, T.-L.; Wang, W.; Weiss, C. D. Establishment of a well-characterized SARS-CoV-2 lentiviral pseudovirus neutralization assay using 293T cells with stable expression of ACE2 and TMPRSS2. *PLoS One* **2021**, *16* (3), e0248348.
(20) Muik, A.; Wallisch, A.-K.; Sänger, B.; Swanson, K. A.; Mühl, J.; Chen, W.; Cai, H.; Maurus, D.; Sarkar, R.; Türeci, Ö. Neutralization of SARS-CoV-2 lineage B. 1.1. 7 pseudovirus by BNT162b2 vaccine–elicited human sera. *Science* **2021**, *371* (6534), 1152-1153.
(21) Xu, Z.; Zou, Y.; Gao, X.; Niu, M.-M.; Li, J.; Xue, L.; Jiang, S. Dual-targeting cyclic peptides of receptor-binding domain (RBD) and main protease (Mpro) as potential drug leads for the treatment of SARS-CoV-2 infection. *Front. Pharmacol.* **2022**, 1041331.
(22) Abel, S. D.; Baird, S. K. Honey is cytotoxic towards prostate cancer cells but interacts with the MTT reagent: Considerations for the choice of cell viability assay. *Food Chem.* **2018**, *241*, 70-78.
(23) Puelles, V. G.; Lütgehetmann, M.; Lindenmeyer, M. T.; Sperhake, J. P.; Wong, M. N.; Allweiss, L.; Chilla, S.; Heinemann, A.; Wanner, N.; Liu, S. Multiorgan and renal tropism of SARS-CoV-2. *N. Engl. J. Med.* **2020**, *383* (6), 590-592.
(24) Schurink, B.; Roos, E.; Radonic, T.; Barbe, E.; Bouman, C. S.; de Boer, H. H.; de Bree, G. J.; Bulle, E. B.; Aronica, E. M.; Florquin, S. Viral presence and immunopathology in patients with lethal COVID-19: a prospective autopsy cohort study. *Lancet Microbe* **2020**, *1* (7), e290-e299.
(25) Gordon, D. E.; Jang, G. M.; Bouhaddou, M.; Xu, J.; Obernier, K.; White, K. M.; O'Meara, M. J.; Rezelj, V. V.; Guo, J. Z.; Swaney, D. L. A SARS-CoV-2 protein interaction map reveals targets for drug repurposing. *Nature* **2020**, *583* (7816), 459-468.